Strategies to improve photosynthetic nitrogen-use efficiency with no yield penalty: lessons from late-sown winter wheat

Running title: Strategies to improve photosynthetic nitrogen-use efficiency

Lijun Yin[a], Haicheng Xu[b], Shuxin Dong[a], Jinpeng Chu[a], Xinglong Dai[a*], Mingrong He[a]*

[a] Collaborative Innovation Team of Shandong Wheat-Corn Crops; National Key Lab. of Crop Biology, Key Lab. of Crop Ecophysiology and Farming System, Ministry of Agriculture, Agronomy College of Shandong Agricultural University, Tai'an 271018, Shandong, P.R. China.

[b] Yellow River Delta Agricultural Hi-tech Industrial Demonstration Zone, Guangbei Farm Zhongxin Street 19, Dongying, Shandong, P.R. China.

*Corresponding author. Tel: +86 05388244018

E-mail addresses: yinlijun326@163.com (Lijun Yin); xuhaich@126.com (Haicheng Xu); dongshuxin666666@163.com (Shuxin Dong); chuJP@sdau.edu.cn (Jinpeng Chu); adaisdny@163.com (Xinglong Dai), mrhe@sdau.edu.cn (Mingrong He).

Highlight

Optimal *N* allocation at several integration levels accounts for improved canopy *PNUE* while maintaining high grain yield in winter wheat

Abstract

Improving canopy photosynthetic nitrogen-use efficiency (*PNUE*) may maintain or even increase yield with reduced *N* input. In this study, later-sown winter wheat was studied to reveal the mechanism underlying improved canopy *PNUE* while maintaining high yield. *N* allocation at several levels was optimised in late-sown wheat plants. *N* content per plant increased. Increased *N* was allocated to the flag leaf and second leaf, and to ribulose-1, 5-bisphosphate carboxylase/oxygenase (*Rubisco*) in upper leaves. Constant or reduced *N* was allocated to leaf 3, leaf 4, and *Rubisco* in lower leaves. The specific green leaf area nitrogen (*SLN*) of upper leaves increased, while that of lower leaves remained unchanged or decreased. *N* allocation to the cell wall decreased in all leaves. As a result, the maximum carboxylation rate of upper leaves increased, and

that of lower leaves remained constant or decreased. CO_2 diffusion capacity was enhanced in all leaves. Outperformance by light-saturated net photosynthetic rate (P_{max}) over *SLN* led to improved *PNUE* in upper leaves. Enhanced P_{max} coupled with unchanged or decreased *SLN* resulted in improved *PNUE* in lower leaves. High yield was maintained because enhanced photosynthetic capacity at the leaf and whole plant levels compensated for reduced canopy leaf area.

Keywords

Leaf mass per area, Light-saturated net photosynthetic rate, *N* allocation, Photosynthetic nitrogen-use efficiency, Specific green leaf area nitrogen, Winter wheat

Abbreviations

C_c, chloroplastic CO_2 concentration
C_i, intercellular CO_2 concentration
ETR, total electron transport rate
g_m, mesophyll conductance
g_s, stomatal conductance
J_{max}, light-saturated potential rate of electron transport
LMA, leaf mass per area
N_m, the mass of nitrogen in the leaf per total mass of leaf
P_{max}, light-saturated net photosynthetic rate
PPFD, photosynthetic photon flux density
PNUE, photosynthetic nitrogen-use efficiency
Rubisco, ribulose-1, 5-bisphosphate carboxylase/oxygenase
R_F, nitrogen allocated to *Rubisco*
SLN, specific green leaf area nitrogen
V_{cmax}, maximum carboxylation rate

Introduction

Wheat (*Triticum aestivum* L.) provides 20% of the calories and protein consumed by humans (Reynolds *et al.*, 2012). An increase in crop yield by 70% is needed if we are to meet the projected demand for food

by 2050 (Tilman *et al.*, 2011; Ray *et al.*, 2013). The amount of nitrogen (*N*) applied will increase with the growing demand for food production in the future (Li *et al.*, 2017). Increased economic costs and environmental concerns have heightened the desire to reduce crop *N* input while maintaining or even increasing grain yield (Cassman *et al.*, 2003; Davidson *et al.*, 2015; Zhang *et al.*, 2015). Therefore, improving *N*-use efficiency (*NUE*) has become a top priority for crop improvement. *NUE* is defined as grain yield per unit of *N* available (from soil and/or fertiliser) and can be further divided into *N*-uptake efficiency and *N*-utilisation efficiency (*UTE*) (Moll *et al.*, 1982). *UTE*, defined as grain yield per unit of *N* taken up, is an important parameter for determining the efficiency with which crop plants utilise *N* to achieve growth and grain yield (Foulkes *et al.*, 2009).

At the end of the 1970s, the concept of plant *N* productivity, defined as the increase in plant dry matter per unit time and per unit *N* content, was introduced to interpret the dependency of plant growth on internal *N* (Ingestad *et al.*, 1979). Following Lambers *et al.* (1990) and Garnier *et al.* (1995), plant *N* productivity was expressed as the product of *N* allocation to leaves within the plant and photosynthetic *N* use efficiency (*PNUE*). The latter was defined as the ratio between photosynthetic rate and *N* concentration in leaves. As most of the grain dry matter at maturity in wheat is contributed by photosynthates produced by leaves during the post-anthesis stage (Roberto *et al.*, 2010; Carmo-Silva *et al.*, 2017), *UTE* at the whole-plant level is dependent on *N* allocation to leaves and the *PNUE* of leaves during the post-anthesis stage.

Plants change *N* allocation to maximise their carbon assimilation at several integration levels. First, they allocate a given amount of *N* over a small or a large plant population through trade-offs between plant density per unit of land and *N* content in individual plants. Second, they change the fraction of *N* invested in leaves, stems and roots. Third, they modulate leaf area per unit *N* invested in leaves by altering their anatomy. Fourth, they change the relative investment of *N* among photosynthetic components. Small changes in *N* allocation can greatly affect the light-saturated photosynthetic rate (P_{max}) and *PNUE*, and therefore plant performance (Feng *et al.*, 2009).

Strategies to improve *PNUE* have been proposed for many species (Poorter *et al.*, 1998; Davey *et al.*, 1999; Pang *et al.*, 2014; Rotundo *et al.*, 2016). Most studies have proposed that the potential benefit of increased photosynthetic capacity for *PNUE* can be realised only when it is not associated with increases in leaf mass per area (*LMA*, g m^{-2}) or specific leaf *N* content (*N* content per unit leaf area, *SLN*), as an increase in *LMA* positively affects *SLN* and therefore reduces *PNUE* (Field and Mooney, 1986; Hirose *et al.*, 1994; Hikosaka *et al.*, 1995; Boote *et al.*, 2003; Anand *et al.*, 2007). However, a strategy that results in lower *SLN* may limit crop yield under some conditions, particularly those designed to produce high yields. Actually, previous studies have suggested that *N* remobilisation from vegetative tissues may be

essential as a mobilisable *N* reservoir to sustain grain yield in cereal crops (Horton, 2000; Barbottin *et al.*, 2005). The amount of *N* accumulated at anthesis largely determines the amount of *N* remobilised during grain filling (Martre *et al.*, 2003; Pask *et al.*, 2012). Taken together, these findings suggest that alternative approaches need to be explored to improve *PNUE* while maintaining high or even increasing grain yield.

Interspecific or intraspecific variations in *PNUE* have been explained by differences in the fraction of light absorbed by the leaf, CO_2 partial pressure at the intercellular space or at carboxylation sites within chloroplasts, *N* allocation to photosynthetic versus non-photosynthetic functions, *N* partitioning between light harvesting complexes, electron transport and CO_2 fixation, activation state or specific activity of ribulose-1, 5-bisphosphate carboxylase/oxygenase (*Rubisco*), respiration in the light, and *SLN* (Field and Mooney, 1986; Evans *et al.*,1989; Quick *et al.*, 1991; Lambers *et al.*, 1992; Pons *et al.*, 1994; Zhu *et al.*, 2007).

Global warming over past decades has provided an additional growing period prior to wintering that has encouraged farmers to delay the winter wheat sowing date (Xiao *et al.*, 2013, 2015). Previous studies have indirectly suggested that delayed sowing of winter wheat may have advantages in crop productivity as a function of plant *N* use (Widdowson *et al.*, 1987; Ehdaie *et al.*, 2001; Weiss *et al.*, 2003; Sun *et al.*, 2007; Jalota *et al.*, 2013; Ding *et al.*, 2016; Rasmussen *et al.*, 2016). Our recent study suggested that delayed sowing improves *UTE* while maintaining a high yield by increasing spike grain weight with fewer spikes per unit area (Yin *et al.*, 2018), suggesting concurrent improvement in *PNUE* and grain productivity at the whole-plant level. The following questions have arisen from these results: (i) What causes late-sown wheat plants to have a higher *PNUE*? (□) How is coupling between improvement in *PNUE* at the whole-plant level and high grain yield at the canopy level achieved? To answer these questions, photosynthetic traits in plants, such as leaf gas exchange, chlorophyll fluorescence, *Rubisco* catalytic properties, and CO_2 diffusion capacity, were investigated along with *N* allocation at the canopy, whole-plant, leaf, and cellular levels. Our main goal was to test the hypothesis that optimal N allocation at several integration levels improves *PNUE* and grain productivity at the whole-plant level, which in turn results in improved canopy *PNUE* while maintaining high yield.

Materials and methods

Plant material and growing conditions

Tainong 18, a widely planted winter wheat cultivar, was grown in the field at the experimental station of Shandong Agricultural University, Taian, Shandong, China during the 2015–2016 and 2016–2017 growing seasons. The preceding crop was summer maize. The soil was sandy loam with a pH of 8.0. The

133 contents of organic matter (Walkley and Black method), total *N* (semi-micro Kjeldahl method), available
134 phosphorus (*P*; Olsen method), and available potassium (*K*; Dirks–Sheffer method) in the 0–20-cm soil
135 layer were 12.0, 1.0, 25.1, and 47.0 mg kg^{-1} during 2015–2016 and 12.1, 1.0, 25.3, and 47.1 mg kg^{-1}
136 during 2016–2017, respectively. Rainfall levels during the growing seasons of 2015–2016 and 2016–2017
137 were 144.9 and 168.3 mm, respectively.
138 Seeds were sown at a density of 405 plants m^{-2}, the optimal planting density of Tainong 18 for higher
139 yield and *NUE* (Dai *et al.*, 2013), in 2015 and 2016 on 8 October (normal sowing) and 22 October (late
140 sowing) using a 12-row planter with 0.25-m row spacing. The cumulative temperature values (sum of
141 daily average air temperature) prior to wintering of the normal and late-sown treatments were 679.4 and
142 444.5°C d during the 2015–2016 growing season and 682.4 and 449.5°C d during the 2016–2017
143 growing season, respectively. The plots were arranged in a completely random design with three
144 replicates. The size of each subplot was 20.0 × 3.0 m. Basal fertilisation of each subplot included *N* as
145 urea, *P* as calcium superphosphate, and *K* as potassium chloride at rates of 120 kg ha^{-1} *N*, 80 kg ha^{-1} P_2O_5,
146 and 120 kg ha^{-1} K_2O, respectively. An additional 120 kg ha^{-1} *N* as urea was applied at the beginning of the
147 jointing stage. Irrigation was carried out before wintering, at jointing, and at anthesis, with approximately
148 60 mm each time. Pests and diseases were controlled chemically. No significant incidences of pests,
149 diseases, or weeds occurred in any of the subplots.
150
151 *Crop measurement*
152 *Biomass and nitrogen content of individual plant and leaves*
153 Plants on 0.2 m^2 were taken as samples and counted in each subplot at 7-day intervals from anthesis to
154 maturity. All individual plants were divided into flag leaf, second leaf, leaf 3, leaf 4, and the remaining
155 parts. The planar green area of each leaf was measured (in cm^{-2}) using a green area meter (Li-Cor 3100,
156 Li-Cor, Inc., Lincoln, NE, USA). Biomass was measured after oven drying to constant mass at 75°C. The
157 samples were ground, and *N* mass per unit dry mass was determined using an elemental analyser (Rapid
158 N Exceed, Elementar, Langenselbold, Germany). The *LMA* (g m^{-2} green leaf area) and *SLN* (g *N* m^{-2} green
159 leaf area) values were calculated.
160
161 *Grain yield, yield components, plant N productivity, and UTE*
162 Plants were harvested from a 2.0-m × 6-row (1.5 m) quadrat in each subplot as described by Dai *et al.*
163 (2013). The grain was air-dried, weighed, and adjusted to standard 12% moisture content (88% dry matter,
164 kg ha^{-1}). This was considered grain dry matter yield.
165 Plant *N* productivity was defined as the increase in plant dry matter per unit time and per unit *N* content.

166 *UTE* was defined as grain yield per unit of *N* taken up (Moll *et al.*, 1982).
167
168 *Biomass and nitrogen content of the cell wall*
169 Biomass and nitrogen content of the cell wall were measured according to the procedures described by
170 Lamport (1965) and Onoda *et al.* (2004). Approximately 10 mg of freeze-dried leaves was extracted in
171 1.5 mL of buffer (50 mm tricine, pH 8.1) containing 1% PVP40 (average molecular weight 40,000,
172 product no. 1407; Sigma Chemical Co., St Louis, MO, USA). The sample was vortexed and centrifuged
173 at 12,000 *g* for 5 min (AG 5424; Eppendorf, Hamburg, Germany), and the supernatant was carefully
174 removed. The pellet was resuspended in buffer without PVP containing 1% sodium dodecyl sulphate
175 (SDS), incubated at 90°C for 5 min and centrifuged at 12,000 *g* for 5 min. This was repeated, and then
176 two washes with 0.2 m KOH, two washes with deionised water, and then two washes with ethanol were
177 carried out. The tube containing the pellet was oven-dried at 80°C. The remaining dry mass of the pellet
178 was assumed to represent the leaf cell wall biomass, and *N* content was determined on 2–5 mg of material
179 using the elemental analyser.
180
181 *Biomass and Rubisco nitrogen content*
182 The *Rubisco* content of each layer leaf at anthesis was determined according to Makino *et al.* (1985,
183 1986). Briefly, leaves were sampled and immersed in liquid *N* and then stored at −70°C. A 0.5-g aliquot
184 of leaves was ground in a buffer solution containing 50 mM Tris-HCl (pH 8.0), 5 mM β-mercaptoethanol,
185 and glycerol 12.5% (v/v), and the extracts were centrifuged for 15 min at 1,500 *g* at 2°C. The supernatant
186 was mixed with dissolving solution containing 2% (w/v) SDS, 4% (v/v) β-mercaptoethanol, and 10% (v/v)
187 glycerol, and the mixture was boiled in water for 5 min for the protein electrophoresis assay. An
188 electrophoretic buffer system was used with sodium dodecyl sulphate–polyacrylamide gel electrophoresis
189 in a discontinuous buffer system with a 12.5% (w/v) separating gel and a 4% (w/v) concentrated gel. The
190 gels were washed with deionised water several times, dyed in 0.25% Coomassie Blue staining solution
191 for 12 h, and decolourised until the background was colourless. Large subunits and relevant small
192 subunits were transferred to a 10-ml cuvette with 2 ml of formamide and washed in a 50°C water bath at
193 room temperature for 8 h. The wash solution was measured at 595 nm using background glue as the blank
194 and bovine serum albumin as the standard protein. Because the amount of *N* per unit *Rubisco* is 16%
195 (Field and Mooney, 1986), *Rubisco N* content per unit leaf area was calculated as *Rubisco* content
196 multiplied by 16%.
197
198 *Relative amount of mRNA*

Total *RNA* was extracted from frozen leaf discs using Trizol according to the manufacturer's specifications. *RNA* yield was determined using a NanoDrop 2000 spectrophotometer (Thermo Scientific, Waltham, MA, USA), and integrity was evaluated by agarose gel electrophoresis and ethidium bromide staining.

A two-step reaction process of reverse transcription and polymerase chain reaction (PCR) was used for quantification. Each reverse transcription reaction had two steps. The first step was 0.5 μg *RNA*, 2 μl of 4 × g *DNA* wiper Mix and 8 μl of nuclease-free H_2O. Reactions were performed in a GeneAmp® PCR System 9700 (Applied Biosystems, Foster City, CA, USA) for 2 min at 42°C. The second step was to add 2 μl of 5× HiScript II Q reverse transcription SuperMix IIa. Reactions were performed in a GeneAmp® PCR System 9700 for 10 min at 25°C, 30 min at 50°C, and 5 min at 85°C. The 10 μl of reverse transcription reaction mix was diluted ×10 in nuclease-free water and held at −20°C. Real-time PCR was performed using the LightCycler® 480 II Real-time PCR instrument (Roche, Basel Switzerland) with 10 μl of PCR reaction mixture that included 1 μl of cDNA, 5 μl of 2× QuantiFast® SYBR® Green PCR Master Mix (Qiagen, Hilden, Germany), 0.2 μl of forward primer, 0.2 μl of reverse primer and 3.6 μl of nuclease-free water. Reactions were incubated in a 384-well optical plate (Roche) at 95°C for 5 min, followed by 40 cycles of 95°C for 10 s and 60°C for 30 s. Each sample was run in triplicate for the analysis. At the end of the PCR cycle, a melting curve analysis was performed to validate specific generation of the expected PCR product. The primer sequences were designed in the laboratory and synthesised by Generay Biotech (Generay, PRC) based on the *mRNA* sequences obtained from the NCBI database as follows: AGTAGCTGCCGAATCTTCT.

The expression levels of *mRNAs* were normalised to GAPDH and were calculated using the $2^{-\Delta\Delta Ct}$ method (Livak and Schmittgen, 2001).

Activated and inactivated Rubisco content

Initial and total *Rubisco* activities were determined according to a procedure described by Keys and Parry (1990). Initial activity was determined by adding 25 μl of supernatant to 475 ml of a CO_2-free assay buffer containing 100 mM bicine, pH 8.2, and 20 mM $MgCl_2$, to which $NaH^{14}CO_3$ (7.4 kBq μmol^{-1}) and *RuBP* had been added to concentrations of 10 and 0.4 mM, respectively, immediately prior to adding the extract. Total activity was determined by incubating 20 ml of extract for 3 min in 980 ml of the same assay buffer without *RuBP*, allowing for carbamylation of all available active sites. The assay was started by adding 0.4 mM *RuBP* as indicated above. The *Rubisco* activation state was determined from the ratio of initial to total activity. The inactive *Rubisco* content was the difference between the total amount of *Rubisco* and active *Rubisco* content.

232

233 *Leaf gas-exchange and fluorescence measurements*

234 Thirty culms with the same flowering date were tagged at anthesis. Gas-exchange measurements were
235 conducted at intervals of 7 days from anthesis to maturity. The leaf light-saturated net photosynthetic rate
236 (P_{max}), stomatal conductance (g_s), and intercellular CO_2 concentration (C_i) of six tagged plants per plot
237 were determined simultaneously. The average P_{max} values of the six plants in each plot were taken as a
238 replicate. P_{max} was measured from 9:00 to 11:00 using a portable photosynthesis system (Li6400; LI-
239 COR) at a light intensity of 1,200 μmol m^{-2} s^{-1}. Leaf temperature during the measurements was
240 maintained at 27.0 ± 0.1°C. The ambient CO_2 concentration in the leaf chamber (C_{a-c}) was adjusted as the
241 atmospheric CO_2 concentration (C_a) (410 ± 1.5 μmol CO_2 mol^{-1}), and relative humidity was maintained at
242 60%. Data were recorded after equilibration to a steady state (~10 min). *PNUE* was calculated by
243 dividing P_{max} by *SLN*.

244 Steady-state fluorescence (F_s), dark-adapted minimum fluorescence (F_o), dark-adapted maximum
245 fluorescence (F_m), and light-adapted maximum fluorescence (F_m') were simultaneously measured using a
246 portable fluorescent instrument (FMS-2, Hansatech, King's Lynn, UK). Data were recorded after
247 equilibration to a steady state. The maximum capture efficiency of excitation energy by open photosystem
248 (PS)II reaction centres (F_v/F_m) and actual capture efficiency of excitation energy by open PSII reaction
249 centres (F_v'/F_m') were estimated according to Genty *et al.* (1989).

250

251 *Measurement of mitochondrial respiration rate in the light (R_d) and the CO_2 compensation point related*
252 *to C_i (Γ^*)*

253 R_d and Γ^* were measured by the following steps, which utilised the photorespiration rate being dependent
254 on and R_d being independent of photosynthetic photon flux density (*PPFD*, reviewed by Brooks and
255 Farquhar, 1985; Bernacchi *et al.*, 2001). When the P_{max}/C_i response curves were prepared at a series of
256 CO_2 concentrations and at a battery of *PPFD*s, they intersected at one point where P_{max} was the same at
257 different *PPFD*s. Therefore, P_{max} at that point represented $-R_d$, and C_i represented Γ^*. In the present
258 experiment, R_d and Γ^* were measured on different leaf layers from 0:00 h to 4:00 h (Brooks and Farquhar,
259 1985; Guo *et al.*, 2005, 2007). *PPFD*s were controlled as a series of 150, 300, and 600 μmol photons m^{-2}
260 s^{-1}. At each *PPFD*, C_{a-c} was adjusted as a series of 25, 50, 80 and 100 μmol CO_2 mol^{-1}. The leaves were
261 fixed in a leaf chamber with a *PPFD* of 600-μmol photons m^{-2} s^{-1} and a C_{a-c} of 100-μmol CO_2 mol^{-1} 30
262 min prior to initiating measurements.

263

264 *Stomatal density and stomatal aperture*

Epidermal peels were stripped from leaves. Stomatal density was recorded under a microscope (Olympus Corp., Tokyo, Japan) in a 0.196-mm^2 leaf area. A total of 1,000 stomatal apertures were measured under the microscope.

Electron microscopy

Approximately 1–2-mm^2 leaf sections were cut from the middle of each layer of leaves at anthesis using two razor blades, fixed in 2.5% glutaraldehyde (0.1 M phosphate buffer, pH 7.4), and post-fixed in 2% osmium tetroxide. Specimens were dehydrated in a graded acetone series and embedded in Epon 812. The leaf sections were cut on a Power Tome-XL ultramicrotome and stained with 2% uranyl acetate,. Then, cell wall thickness, chloroplast number, and chloroplast size were examined with an H-7650 transmission electron microscope.

Calculation

Calculation of ETR: Total electron transport rate (*ETR*) was calculated from Eq. 1:

$$ETR = (Fm' - Fs)/Fm' \times PPFD \times \alpha_{leaf} \times \beta, \quad (1)$$

where α_{leaf} is leaf absorbance, and β is the distribution of electrons between PSI and PSII. α_{leaf} is dependent on chlorophyll content, and a curvilinear relationship between leaf absorption and chlorophyll content was observed by Evans (Evans *et al.*, 1996; Evans and Poorter, 2001). However, curvature was extremely low when chlorophyll content was >0.4 mmol m^{-2}. According to Evans and Poorter (2001), the α_{leaf} calculation demonstrates that α_{leaf} is close to 0.85 (Asner *et al.*, 1998; Manter and Kerrigan, 2004). In this study, α_{leaf} was also assumed to be 0.85, and β was assumed to be 0.5 (Ehleringer and Pearcy, 1983; Alvertssom, 2001).

Calculation of V_{cmax}: The V_{cmax} was calculated as described by Wilson *et al*. (2000).

$$V_{cmax} = 6.25 \times V_{cr} \times LMA \times N_m \times R_{F,} \quad (2)$$

where 6.25 is the ratio of the weight of *Rubisco* to the weight of *N* in *Rubisco*; V_{cr} is the specific activity of *Rubisco*, which is assumed to be only a function of temperature (20.7 μmol CO_2 (g *Rubisco*)$^{-1}$ s^{-1} at 25°C); *LMA* is leaf mass per unit area (g m^{-2}); N_m (g g^{-1}) is the mass of *N* in the leaf per total mass of leaf; and R_F is the apparent fraction of that *N* allocated to *Rubisco*.

Calculation of C_c and g_m: Carbon dioxide concentration in chloroplasts (C_c) and mesophyll conductance (g_m) were calculated from Eqs. 6 and 7 (Harley *et al.*, 1992; Epron *et al.*, 1995; Manter and Kerrigan, 2004):

$$C_c = \{\Gamma^* [ETR + 8(P_{max} + R_d)] / [ETR - 4(P_{max} + R_d)]\}, \quad (3)$$

$$P_{max} = g_m \times (C_i - C_c), \quad (4)$$

where ETR and P_{max} were obtained from the gas-exchange and chlorophyll *a* fluorescence measurements conducted under saturating light; R_d and Γ^* were estimated as described above.

Statistical analysis

Our results were analysed using DPS v 7.05 software (Hangzhou RuiFeng Information Technology Co., Ltd., Hangzhou, Zhejiang, China). Multiple comparisons were made after a preliminary F-test. Means were tested based on the least significant difference at $P < 0.05$.

Results

N allocation at the canopy level, plant N productivity, grain yield, and UTE

Over two wheat growing seasons, late-sown wheat plants accumulated less *N* per unit area than did that sown on the normal sowing date (Fig. 1). These reduced amounts of *N* were spread to a smaller plant population (Table 1) with higher *N* content in individual plants (Fig. 2). The above-ground biomass and *N* uptake (*AGN*) per unit area at anthesis were both reduced when the sowing date was delayed from 8 to 22 October (Fig. 1). As a result, similar plant *N* productivity was obtained from sowing to anthesis on both sowing dates. Late-sown wheat plants also accumulated less *AGN* from anthesis to harvest, but more biomass per unit area than did those with the normal sowing date. An average 30.8% increase in plant *N* productivity was obtained from anthesis to harvest under the later sowing date over the normal sowing date for the two wheat growing seasons (Fig. 1), indicating that improved plant *N* productivity with delayed sowing mainly resulted from more efficient *N* use during the post-anthesis period.

A high grain yield of >9,000 kg ha^{-1} was maintained, and *UTE* at harvest increased significantly when the sowing date was delayed (Table 1). In general, spike number per unit area decreased and spike grain weight increased as a result of increased spike grain number and unchanged grain weight (Table 1). These

results suggest that trade-offs between spike number per unit area and grain number per spike resulted in similar grain yields between the two sowing dates.

N allocation at the levels of the whole-plant and leaf, LMA, SLN, P_{max}, and PNUE

With increased *AGN* and biomass of individual plants (Fig. 2), later-sown wheat plant allocated higher fractions of *AGN* and biomass at anthesis to the upper leaves, including the flag leaves and second leaves. The fraction of *AGN* and biomass allocated to lower-position leaves, including leaves 3 and 4, remained constant or decreased (Fig. 3). Different responses to delayed sowing in *LMA* and *SLN* were observed with leaf position in the canopy, as the area of all positioned leaves was not affected (Fig. 4). The *LMA* and *SLN* of the upper leaves increased, and those of lower positioned leaves remained constant or decreased (Fig. 5). The N_m of all leaves remained unchanged. Therefore, changes in *SLN* were almost completely dependent on *LMA*.

Improvement in P_{max} and *PNUE* was attained in all leaves with delayed sowing. When the sowing date was delayed from 8 to 22 October, P_{max} at anthesis increased over two growing seasons by, on average, 21.5%, 30.6%, 14.5%, and 25.4% in flag leaves, second leaves, and leaves 3 and 4, respectively (Fig. 6). Overall mean *PNUE* values at anthesis over the two growing seasons increased by 18.5%, 16.1%, 20.9%, and 31.2% in flag leaves, second leaves, leaf 3, and leaf 4, respectively (Fig. 6). The *PNUE* performance of the post-anthesis stage in different leaf layers was similar to that of anthesis (Supplemental Fig. 1).

Taken together, these results suggest that strategies underlying improvements in *PNUE* in flag leaves and second leaves differed from that in leaves 3 and 4. Increased P_{max} coupled with higher *LMA* and *SLN* in flag leaves and second leaves contributed to improve *PNUE*, whereas the combination of constant or reduced *SLN* and enhanced photosynthetic capability in leaves 3 and 4 resulted in improved *PNUE*.

N allocation at the cellular level, Rubisco catalytic properties, and CO_2 diffusion capacity

Optimising the functionality of *Rubisco* has large implications for improved plant productivity and resource use efficiency. Position-specific changes in transcript levels of the *mRNAs* coding *Rubisco* (Fig. 7) and the amount of *Rubisco* expressed as biomass and *N* content on a unit leaf area basis (Fig. 8) were observed with delayed sowing. As the allocation proportion of biomass and *N* to the cell wall decreased, the biomass and *N* content in the cell wall on a unit leaf area basis decreased for all positioned leaves (Fig. 8). The proportion of biomass and *N* allocated to total *Rubisco* and activated *Rubisco* in the flag and second leaves increased, while those in leaves 3 and 4 remained unchanged or decreased after the sowing date was delayed (Fig. 9). The V_{cmax} of the upper leaves increased, and that in the lower leaves remained constant or decreased (Fig. 10).

364 Diffusional conductance of CO_2 is the diffusive physiological determinant for the CO_2 concentration at
365 the *Rubisco* carboxylation site that directly affects net photosynthetic rate by limiting the amount of
366 substrate (CO_2) for fixation. The g_s, g_m, and associated traits, such as the number of stomata per unit area,
367 stomatal aperture, cell wall thickness, chloroplast number, intercellular CO_2 concentration, and
368 chloroplast CO_2 concentration, were measured or estimated. Higher g_s values were obtained in leaves at
369 all positions with later sowing compared with normal sowing, resulting in higher intercellular CO_2
370 concentration (C_i) (Fig. 11), which was associated with increased stomatal number per unit area (Fig. 12)
371 and unchanged stomatal aperture. The g_m values in all leaves at all positions were also enhanced by
372 delayed sowing; consequently, higher chloroplast CO_2 concentration (C_c) was obtained (Fig. 11). The
373 main reasons for this boosted g_m include decreased cell wall thickness (Figs. 13, 14), increased
374 chloroplast number per unit leaf area (Fig. 13), and unchanged chloroplast size in response to delayed
375 sowing.
376
377 **Discussion**
378
379 Manipulating *PNUE* at the leaf or whole-plant level will only be beneficial if it confers an improvement
380 at the crop canopy level. As shown by Townsend *et al.* (2017), there is an opportunity to improve *PNUE*
381 in the wheat canopy with no detriment to carbon gain or grain protein content by reducing the level of
382 canopy *N*. In the present study, reduced canopy *AGN* at anthesis and at harvest were observed in response
383 to delayed sowing. Later-sown wheat plants produced more biomass and grain yield on a unit area basis
384 from anthesis to harvest with less *N* consumption than did those sown at a normal date, resulting in
385 improved *PNUE* at the whole-plant level and *UTE* taking a reduced number of plants per unit area into
386 consideration. As reduced total crop leaf area resulting from fewer plants per unit area was compensated
387 for by enhanced photosynthetic capacity at the leaf and whole-plant levels, an improvement in *PNUE* at
388 the crop canopy level was obtained while high grain yield was maintained.
389 It has long been recognised that the upper leaves serve as a major contributor to photoassimilates in the
390 wheat grain (Waters *et al.*, 1980; Simpson *et al.*, 1983; Lopes *et al.*, 2006), while lower leaves contribute
391 relatively little to grain yield during the grain-filling stage. Individual leaves require progressively less *N*
392 from the top to the bottom of a canopy to maximise carbon assimilation (Gastal and Lemaire, 2002). Thus,
393 an optimal correlation between the distribution of photosynthetic capacity, light, and *SLN* in flag leaves
394 and second leaves is the main target for gains in yield potential, whereas leaves 3 and 4 are the main
395 targets for gains in *PNUE* (Townsend *et al.*, 2018). In the present study, *AGN* at anthesis increased in
396 individual plants due to a reduced number of plants per unit area. Leaf position-specific changes in *N*

allocation were observed. *N* allocation to the upper leaves, such as the flag leaf and second leaf, increased, while *N* allocation to lower leaves, such as leaves 3 and 4, remained unchanged or decreased.

Canopy-level *PNUE* is a complex trait involving many plant characteristics and processes from leaf anatomy and composition to leaf physiology. Earlier studies concluded that increasing *PNUE* without considering grain yield required de-coupling of photosynthetic capacity and *SLN*. Strategies to improve *PNUE* while maintaining or increasing yield are lacking. This could potentially be achieved when P_{max} is improved more than *SLN*.

Leaf conductance of CO_2 and *Rubisco* kinetic parameters play key roles in carbon assimilation that are necessary for a proper understanding of photosynthetic performance under field conditions. High photosynthetic efficiency intrinsically demands tight coordination between traits related to CO_2 diffusion capacity and leaf biochemistry. V_{cmax} is the measure of the process by which *Rubisco* catalyses ribulose-1,5-bisphosphate (*RuBP*) with CO_2 to produce the carbon compounds that eventually become triose phosphates (e.g. glyceraldehyde-3P), the building block for sugars and starches. According to Wilson *et al.* (2000), variations in V_{cmax} can be explained by changes in *LMA*, N_m, and the *N* allocated proportion to *Rubisco* (R_F). In the present study, N_m remained unchanged in all leaves. The *LMA* and R_F values in the flag and second leaves increased in response to delayed sowing, resulting in improved V_{cmax}. However, *LMA* decreased in leaves 3 and 4, while R_F remained unchanged in leaves 3 and 4, leading to unchanged V_{cmax} in leaf 3 and a decrease in V_{cmax} in leaf 4. The parallel increase between *LMA* and R_F disagrees with a previous observation in which smaller *N* partitioning into *Rubisco* was observed against larger *N* partitioning into cell walls with increasing *LMA* (Poorter and Evans, 1998; Onoda *et al.*, 2004; Takashima *et al.*, 2004; Wright *et al.*, 2005; Harrison *et al.*, 2009; Hidaka *et al.*, 2009). The main reason for this difference may be related to whether interspecific (previous study) or intraspecific comparisons were made (present study).

As V_{cmax} represents the maximum carboxylation rate under both light-saturated and CO_2-saturated conditions, P_{max} was measured under light saturation but at a normal ambient CO_2 concentration; therefore, the difference between the two parameters reflected a limitation on photosynthetic capacity exerted by the CO_2 supply.

The g_m value, a limiting factor for CO_2 diffusion to carboxylation sites in the stroma, is usually tightly coregulated with g_s (Flexas *et al.*, 2013). The g_m value depends on the surface area of mesophyll cells exposed to the intercellular air space and the thickness of the mesophyll cell walls (Evans *et al.*, 1994, 2009; Tholen and Zhu, 2011; Tosens *et al.*, 2012). The finding that g_m is constrained by large *LMA* has been reviewed previously (Flexas *et al.*, 2008), and the underlying reason is mostly related to the thicker cell walls observed in species with high *LMA*, which significantly limits CO_2 diffusion inside leaves

(Parkhurst, 1994; Hanba *et al.*, 1999; Wright *et al.*, 2005; Hidaka *et al.*, 2009; Peguero-Pina *et al.*, 2012; Tosens *et al.*, 2012; Tomás *et al.*, 2013). In contrast to previous reports, thinner cell walls in leaves at all positions were observed with larger *LMA* due to reduced biomass allocation to the cell wall under the delayed sowing condition. Moreover, an increase in the number of chloroplasts per unit leaf area allowed for a larger surface area of mesophyll cells exposed to intercellular air space. Higher g_s values were obtained in leaves at all positions on plants sowed later due to an increased number of stomata per unit area and an unchanged stomatal aperture, which is also helpful for increasing chloroplastic CO_2 concentration (C_c). Combining these observations, we propose that the dominant mechanism for improved P_{max} in lower leaves in the canopy is enhanced CO_2 diffusion capacity, and that in the upper leaves is dependent on the combination of *Rubisco* catalytic properties and CO_2 diffusion capacity.

Conclusion

Optimal *N* allocation was achieved at several integration levels in response to delayed sowing. A limited amount of *N* was spread over a reduced plant population at the crop-canopy level, which in turn resulted in increased *N* content in individual plants. An increased fraction of *N* was allocated to upper leaves, including the flag and second leaves, which are main contributors of photoassimilates to grain filling. A decreased fraction of *N* was allocated to lower leaves, including leaves 3 and 4, which contribute relatively little to grain yield during grain filling. At the leaf level, N_m was constant between the two sowing dates. The *LMA* of upper leaves increased as a result of investing more biomass in a given area. As N_m remained constant, the *SLN* of these leaves increased, whereas *LMA* and *SLN* of the lower leaves remained unchanged or decreased. At the cellular level, larger proportions of *N* were allocated to *Rubisco* (both total and activated), which alone or along with increased *LMA* increased V_{cmax} in the upper leaves, while it remained unchanged or decreased in the lower leaves. Higher g_s values were obtained in leaves at all positions with later sowing due to the increased number of stomata per unit area and unchanged stomatal aperture, which is helpful for increasing C_i. Thinner cell walls and an increased number of chloroplasts per unit leaf area allowed for increases in g_m and C_c. Tight coordination between *Rubisco* catalytic properties and CO_2 diffusion capacity led to improved P_{max} in the upper leaves, whereas improvement in P_{max} in lower leaves is dependent on enhanced CO_2 diffusion capacity. Outperformance by P_{max} over *SLN* led to improved *PNUE* in upper leaves. Enhanced P_{max} coupled with unchanged or decreased *SLN* resulted in improved *PNUE* in lower leaves. In summary, optimal *N* allocation accounted for the improvement in *PNUE* at the crop-canopy level while maintaining a high grain yield.

Acknowledge

This work was supported by the Chinese National Basic Research Program (2015CB150404) and Funds of Shandong "Double Top" Program (SYL2017YSTD05).

References

Alvertssom PA. 2001. A quantitative model of the domain structure of the photosynthetic membrane. *Trends in Plant Science* **6,** 349–354.

Anand A, Suresh K, Nair TVR. 2007. Photosynthetic variation and photosynthetic nitrogen use efficiency in Brassica species with different genetic constitution of ribulose-1,5-bisphosphate carboxylase. *Photosynthetica* **45,** 147–152.

Asner GP, Wessman CA, Archer S. 1998. Scale dependence of absorption of photosynthetically active radiation in terrestrial ecosystems. *Ecological Applications* **8,** 1003–1021.

Barbottin A, Lecomte C, Bouchard C, Jeuffroy M-H. 2005. Nitrogen remobilization during grain filling in wheat. *Crop Science* **45,** 1141–1150.

Bernacchi CJ, Singsaas EL, Pimentel C, Portis Jr AR, Long SP. 2001. Improved temperature response functions for models of Rubisco-limited photosynthesis. *Plant, Cell and Environment* **24,** 253–259.

Boote KJ, Jones JW, Batchelor WD, Nafziger ED, Myers O. 2003. Genetic coefficients in the CROPGRO-Soybean model: links to field performance and genomics. *Agronomy Journal* **95,** 32–51.

Brooks A, Farquhar GD. 1985. Effect of temperature on the CO_2/O_2 specificity of ribulose-1, 5-bisphosphate carboxylase/oxygenase and the rate of respiration in the light. *Planta* **165,** 397–406.

Carmo-Silva E, Andralojc PJ, Scales JC, Driever SM, Mead A, Lawson T, Raines CA & Parry MAJ. 2017. Phenotyping of field-grown wheat in the UK highlights contribution of light response of photosynthesis and flag leaf longevity to grain yield. *Journal of Experimental Botany* **68,** 3473–3486.

Cassman KG, Dobermann A, Walters DT, Yang HS. 2003. Meeting cerealdemand while protecting natural resources and improving environmentalquality. *Annual Review of Environment and Resources* **28,** 315–358.

Dai XL, Zhou XH, Jia DY, Xiao LL, Kong HB, He MR. 2013. Managing the seeding rate to improve nitrogen-use efficiency of winter wheat. *Field Crops Research* **154,** 100–109.

Davey PA, Parsons AJ, Atkinson L, Wadge K, Long SP. 1999. Does photosynthetic acclimation to elevated CO_2 increase photosynthetic nitrogen-use efficiency? A study of three native UK grassland species in open-top chambers. *Functional Ecology* **13,** 21–28.

Davidson EA, Suddick EC, Rice CW, Prokopy LS. 2015. More food, low pollution (Mo Fo Lo Po): a grand challenge for the 21st century. *Journal of Environment Quality* **44,** 305–311.

Ding DY, Feng H, Zhao YJ, He Q, Zou YF, Jin JM. 2016. Modifying Winter Wheat Sowing Date as an Adaptation to Climate Change on the Loess Plateau. *Agronomy Journal* **108,** 53–63.

Ehdaie B & Waines JG. 2001. Sowing date and nitrogen rate effects on dry matter and nitrogen partitioning in bread and durum wheat. *Field Crops Research* **73,** 47–61.

Ehleringer J, Pearcy RW. 1983. Variation in quantum yield for CO_2 uptake among C_3 and C_4 plants. *Plant Physiology* **73,** 555–559.

Epron D, Godard D, Cornic G, Genty B. 1995. Limitation of net CO_2 assimilation rate by internal resistances to CO_2 transfer in the leaves of two tree species (Fagus sylvatical L. and Castanea sativa Mill. *Plant, Cell, and Environment* **18,** 43–51.

Evans JR. 1989. Photosynthesis and nitrogen relationships in leaves of C_3 plants. *Oecologia* **78,** 9–19.

Evans JR. 1996. Photosynthesis and the environment. Dordrecht: Kluwer Academic Publishers.

Evans JR, Kaldenhoff R, Genty B, Terashima I. 2009. Resistances along the CO_2 diffusion pathway inside leaves. *Journal of Experimental Botany* **60,** 2235–2248.

Evans JR, von Caemmerer S, Setchell BA, Hudson GS. 1994. The relationship between CO_2 transfer conductance and leaf anatomy in transgenic tobacco with a reduced content of Rubisco. *Australian Journal of Plant Physiology* 2**1,** 475–495.

Evans JR, Poorter H. 2001. Photosynthetic acclimation of plants to growth irradiance: the relative importance of specific leaf area and nitrogen partitioning in maximizing carbon gain. *Plant, Cell, and Environment* **24,** 755–767.

Feng YL, Lei TB, Wang RF, Callaway RM, Valientebanuet A, Inderjit, Li YP, Zheng YL. 2009. Evolutionary tradeoffs for nitrogen allocation to photosynthesis versus cell walls in an invasive plant. *Proceedings of the National Academy of Sciences of the United States of America* **106,** 1853–1856.

Field C & Mooney HA. 1986. The photosynthesis-nitrogen relationship in wild plants. *On the Economy of Form and Function (ed. TJ Givnish)* pp, 25–55. Cambridge University Press, Cambridge, UK.

Flexas J, Diaz-Espejo A, Galmés J, Medrano H. 2008. Mesophyll conductance to CO_2: current knowledge and future prospects. *Plant, Cell and Environment* **31,** 602–621.

Flexas J, Niinemets U, Gallé A, et al. 2013. Diffusional conductances to CO_2 as a target for increasing photosynthesis and photosynthetic water-use efficiency. *Photosynthesis Research* **117,** 45–59.

Foulkes MJ, Hawkesford MJ, Barraclough PB, Holdsworth MJ, Kerr S, Kightley S, Shewry PR. 2009. Identifying traits to improve the nitrogen economy of wheat: Recent advances and future prospects. *Field Crops Research* **114,** 329–342.

Garnier E, Gobin O, Poorter H. 1995. Nitrogen productivity depends on photosynthetic nitrogen use efficiency and on nitrogen allocation within the plant. *Annals of Botany* **76,** 667–672.

Gastal F & Lemaire G. 2002. N uptake and distribution in crops: an agronomical and ecophysiolocal perspective. *Journal of Experimental Botany* **53,** 789–799.

Genty B, Briantais JM, Baker NR. 1989. The relationship between the quantum yield of photosynthetic electron transport and quenching of chlorophyll fluorescence. *BBA-General Subjects* **990,** 87–92.

Guo SW, Schinner K, Sattelmacher B, Hansen UP. 2005. Different apparent CO_2 compensation points in nitrate- and ammonium-grown Phaseolus vulgaris and the relationship to non-photorespiratory CO_2 evolution. *Physiologia Plantarum* **123,** 288–301.

Guo SW, Zhou Y, Shen QR, Zhang F. 2007. Effect of ammonium and nitrate nutrition on some physiological processes of higher plants. *Plant Biology* **9,** 21–29.

Hanba YT, Miyazawa SI, Terashima I. 1999. The influence of leaf thickness on the CO_2 transfer conductance and leaf stable carbon isotope ratio for some evergreen tree species in Japanese warm temperate forests. *Functional Ecology* **13,** 632–639.

Harley PC, Loreto F, Mareo GD, Sharkey TD. 1992. Theoretical considerations when estimating the mesophyll conductance to CO_2 flux by analysis of the response of photosynthesis to CO_2. *Plant Physiology* **98,** 1429–1436.

Harrison MT, Edwards EJ, Farquhar GD, Nicotra AB, Evans JR. 2009. Nitrogen in cell walls of sclerophyllous leaves accounts for little of the variation in photosynthetic nitrogen-use efficiency. *Plant, Cell, and Environment* **32,** 259–270.

Hidaka A & Kitayama K. 2009. Divergent patterns of photosynthetic phosphorus-use efficiency versus nitrogen-use efficiency of tree leaves along nutrient-availability gradients. *Journal of Ecology* **97,** 984–991.

Hikosaka K & Terashima I. 1995. A model of the acclimation of photosynthesis in the leaves of C3 plants to sun and shade with respect to nitrogen use. *Plant, Cell and Environment* **18,** 605–618.

Hirose T & Werger MJA. 1994. Photosynthetic capacity and nitrogen partitioning among species in the canopy of a herbaceous plant community. *Oecologia* **100,** 203–212.

Horton P. 2000. Prospects for crop improvement through the genetic manipulation of photosynthesis: morphological and biochemical aspects of light capture. *Journal of Experimental Botany* **51,** 475–485.

Ingestad T. 1979. Nitrogen stress in birch seedlings. II. N, K, P, Ca, and Mg nutrition. *Physiology Plant* **45,** 149–157.

Jalota SK, Kaur H, Kaur S, Vashisht BB. 2013. Impact of climate change scenarios on yield, water and nitrogen-balance and-use efficiency of rice-wheat cropping system. *Agricultural Water Management* **116,** 29–38.

Keys AJ, Parry MAJ. 1990. Ribulose bisphosphate carboxylase/oxygenase and carbonic anhidrase. *Methods in Plant Biochemistry* **3,** 1–14.

Lambers H, Freijsen N, Poorter H, Hirose T, vander Werf A. 1990. Analyses of growth based on net assimilation rate and nitrogen productivity. Their physiological background. In: Lambers H, Cambridge ML, Konings H, Pons TL, eds. Causes and consequences of variation in growth rate and productivity of higher plants. *The Hague: SPB Academic Publishing by* 1–17.

Lambers H & Poorter H. 1992. Inherent variation in growth rate between higher plants: a search for physiological causes and ecological consequences. *Advances in Ecological Research* **23,** 187–261.

Lamport D. 1965. The protein component of primary cell walls. *Advances in Botanical Research* **2,** 151–218.

Li H, Hu B, Chu CC. 2017. Nitrogen use efficiency in crops: Lessons from Arabidopsis and rice. *Journal of Experimental Botany* **68,** 2477–2488.

Livak KJ and Schmittgen TD. 2001. Analysis of relative gene expression data using real-time quantitative PCR and the 2 (-Delta Delta C(T)) Method. *Methods* **25(4),** 402–408.

Lopes MS, Cortadellas N, Kichey T, Dubois F, Habash DZ, Araus JL. 2006. Wheat nitrogen metabolism during grain filling: comparative role of glumes and the flag leaf. *Planta* **225,** 165–181.

Makino A, Mae T, Chira K. 1985. Photosynthesis and rubulose-1, 5-bisphosphate carboxylase/oxygenase in rice leaves from emergence through senescence. *Planta* **166,** 414–420.

Makino A, Mae T, Chira K. 1986. Colorimetric measurement of protein stained with Coomassie Brilliant Blue R on sodium dodecyl sulfate-polyacrylamide gel electrophoresis by eluting with formamide. *Agricultural and Biological Chemistry* **50,** 1911–1912.

Manter DK, Kerrigan J. 2004. A/C_i curve analysis across a range of woody plant species: influence of regression analysis parameters and mesophyll conductance. *Journal of Experimental Botany* **55,** 2581–2588.

Martre P, Porter JR, Jamieson PD, Triboï E. 2003. Modeling grain nitrogen accumulation and protein composition to understand the sink/source regulations of nitrogen remobilization for wheat. *Plant Physiology* **133,** 1959–1967.

Moll RH, Kamprath EJ, Jackson WA. 1982. Analysis and interpretation of factors which contribute to efficiency of nitrogen utilization. *Agronomy Journal* **74,** 562–564.

Onoda Y, Hikasaka K, Hirose T. 2004. Allocation of nitrogen to cell walls decreases photosynthetic nitrogen-use efficiency. *Functional Ecology* **18,** 419–425.

Pang J, Palta JA, Rebetzke GJ, Milroy SP. 2014. Wheat genotypes with high early vigour accumulate more nitrogen and have higher photosynthetic nitrogen use efficiency during early growth. *Functional Plant Biology* **41,** 215–222.

Parkhurst DF. 1994. Diffusion of CO_2 and other gases inside leaves. *New Phytologist* **126,** 449–479.

Pask AJD, Sylvester-Bradleyb R, Jamiesonc PD, Foulkesa MJ. 2012. Quantifying how winter wheat crops accumulate and use nitrogen reserves during growth. *Field Crops Research* **126,** 104–118.

Peguero-Pina JJ, Flexas J, Galmés J, Sancho-Knapik D, Barredo G, Villarroya D, Gil-Pelegrín E. 2012. Leaf anatomical properties in relation to differences in mesophyll conductance to CO_2 and photosynthesis in two related Mediterranean Abies species. *Plant, Cell, and Environment* **35,** 2121–2129.

Pons T, van der Werf A, Lambers H. 1994. Photosynthetic nitrogen use efficiency of inherently slow- and fast-growing species: possible explanations for observed differences. *In A Whole Plant Perspective on Carbon–Nitrogen Interactions (eds J. Roy & E. Garnier)* pp, 61–77. Academic Publishing, The Hague, the Netherlands.

Poorter H & Evans JR. 1998. Photosynthetic nitrogen-use efficiency of species that differ inherently in specific leaf area. *Oecologia* **116,** 26–37.

Quick WP, Schurr U, Fichtner K, Schulze ED, Rodermel SR, Bogorad L, Stitt M. 1991. The impact of decreased rubisco on photosynthesis, growth, allocation and storage in tobacco plants which have been transformed with antisense rbcS. *Plant Journal* **1,** 51–58.

Rasmussen IS & Thorup-Kristensen K. 2016. Does earlier sowing of winter wheat improve root growth and N uptake? *Field Crops Research* **196,** 10–21.

Ray DK, Mueller ND, West PC, Foley JA. 2013. Yield trends are insufficient to double global crop production by 2050. *Plos One* **8,** e66428.

Reynolds M, Foulkes J, Furbank R, Griffiths S, King J, Murchie E, Parry M, Slafer G. 2012. Achieving yield gains in wheat. *Plant, Cell, and Environment* **35(10),** 1799–1823.

Roberto Ferrise, Andrea Triossi, Pierre Stratonovitch, Marco Bindi, Pierre Martre. 2010. Sowing date and nitrogen fertilization effects on dry matter and nitrogen dynamics for durum wheat: An experimental and simulation study. *Field Crops Research* **117,** 245–257.

Rotundo JL & Borrás L. 2016. Reduced soybean photosynthetic nitrogen use efficiency associated with evolutionary genetic bottlenecks. *Functional Plant Biology* **43,** 462–469.

Simpson RJ, Lambers H, Dalling MJ. 1983. Nitrogen redistribution during grain growth in wheat (Triticum aestivum L.): IV. development of a quantitative model of the translocation of nitrogen to the grain. *Plant Physiology* **71,** 7–14.

Sun H, Zhang X, Chen S, Pei D, Liu C. 2007. Effects of harvest and sowing time on the performance of the rotation of winter wheat-summer maize in the North China Plain. *Industrial Crops and Products* **25,** 239–247.

Takashima T, Hikosaka K, Hirose T. 2004. Photosynthesis or persistence: nitrogen allocation in leaves of evergreen and deciduous Quercus species. *Plant, Cell, and Environment* **27,** 1047–1054.

Tholen D & Zhu XG. 2011. The mechanistic basis of internal conductance: a theoretical analysis of mesophyll cell photosynthesis and CO_2 diffusion. *Plant Physiology* **156,** 90–105.

Tilman D, Balzer C, Hill J, Befort BL. 2011. Global food demand and the sustainable intensification of agriculture. *Proceedings of the National Academy of Sciences of the United States of America* **108,** 20260–20264.

Tomás M, Flexas J, Copolovici L, et al. 2013. Importance of leaf anatomy in determining mesophyll diffusion conductance to CO_2 across species: quantitative limitations and scaling up by models. *Journal of Experimental Botany* **64,** 2269–2281.

Tosens T, Niinemets Ü, Westoby M, Wright IJ. 2012. Anatomical basis of variation in mesophyll resistance in eastern Australian sclerophylls: news of a long and winding path. *Journal of Experimental Botany* **63,** 5105–5119.

Townsend AJ, Retkute R, Chinnathambi K, Randall JW, Foulkes J, Carmo-Silva E, Murchie EH. 2017. Suboptimal acclimation of photosynthesis to light in wheat canopies. *Plant Physiology* **176,** pp.01213.

Waters SP, Peoples MB, Simpson RJ, Dalling MJ. 1980. Nitrogen redistribution during grain growth in wheat (Triticum aestivum L.): I. Peptide hydrolase activity and protein breakdown in the flag leaf, glumes and stem. *Planta* **148,** 422–428.

Weiss A, Hays CJ, Won J. 2003. Assessing winter wheat responses to climate change scenarios: A simulation study in the U.S. Great Plains. *Climatic Change* **58,** 119–148.

Widdowson FV, Penny A, Darby R J, Bird E, Hewitt MV. 1987. Amounts of NO_3-N and NH_4-N in soil, from autumn to spring, under winter wheat and their relationship to soil type, sowing date, previous crop and N uptake at Rothamsted, Woburn and Saxmundham, 1979–85. *Journal of Agricultural Science* **108,** 73–95.

Wilson KB, Baldocchi DD & Hanson PJ. 2000. Quantifying stomatal and non-stomatal limitations to carbon assimilation resulting from leaf aging and drought in mature deciduous tree species. *Tree Physiology* **20,** 787–797.

Wright IJ, Reich PB, Cornelissen JHC, et al. 2005. Assessing the generality of global leaf trait relationships. *New Phytologist* **166,** 485-496.

Xiao D, Moiwo JP, Tao F, Yang Y, Shen Y, Xu Q, Liu J, Zhang H, Liu F. 2015. Spatiotemporal variability of winter wheat phenology in response to weather and climate variability in China. *Mitigation and Adaptation Strategies for Global Change* **20,** 1191–1202.

Xiao D, Tao F, Liu Y, Shi W, Wang M, Liu F, Zhang S, Zhu Z. 2013. Observed changes in winter wheat phenology in the North China Plain for 1981–2009. *International Journal of Biometeorology* **57,** 275–285.

Yin LJ, Dai XL, He MR. 2018. Delayed sowing improves nitrogen utilization efficiency in winter wheat without impacting yield. *Field Crops Research* **221,** 90–97.

Zhang X, Davidson EA, mauzerall DL, searchinger TD, Dumas P, Shen Y. 2015. Managing nitrogen for sustainable development. *Nature* **528,** 51–59.

Zhu XG, de Sturler E, Long SP. 2007. Optimizing the distribution of resources between enzymes of carbon metabolism can dramatically increase photosynthetic rate: a numerical simulation using an evolutionary algorithm. *Plant Physiology* **145,** 513–526.

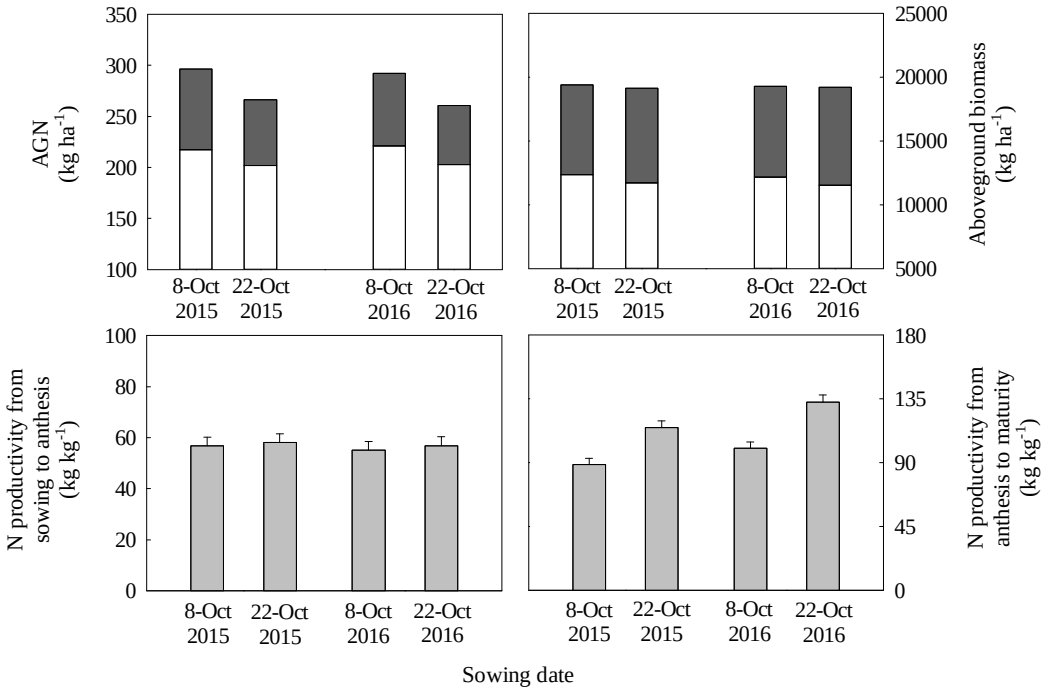

Fig. 1. Aboveground N uptake (*AGN*) at anthesis (blank column) and maturity (blank column plus dark grey column), aboveground biomass at anthesis (blank column) and maturity (blank column plus dark grey column), *N* productivity from sowing to anthesis and from anthesis to maturity of winter wheat over two growing seasons. Vertical bars indicate standard error. Columns as follows: blank, aboveground AGN and biomass at anthesis; black, aboveground AGN and biomass from anthesis to maturity; light grey, N productivity.

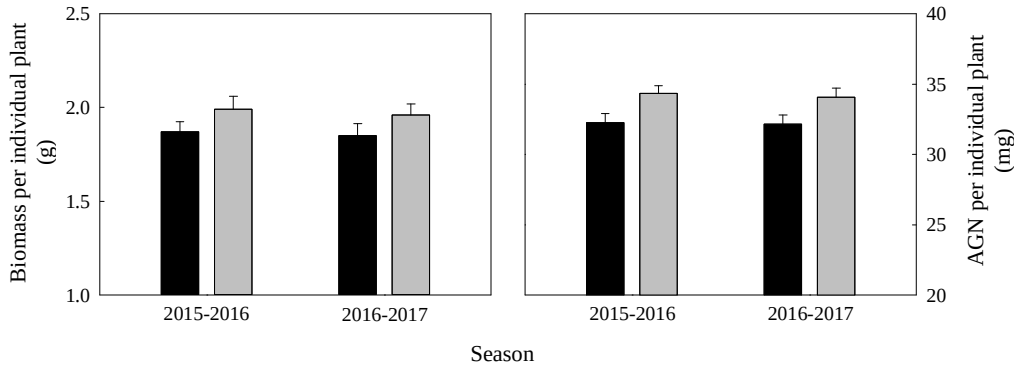

Fig. 2. Biomass and aboveground nitrogen uptake (*AGN*) per individual plant at anthesis in winter wheat over two growing seasons. Vertical bars indicate standard errors. Columns as follows: black, 8 October; dark grey, 22 October.

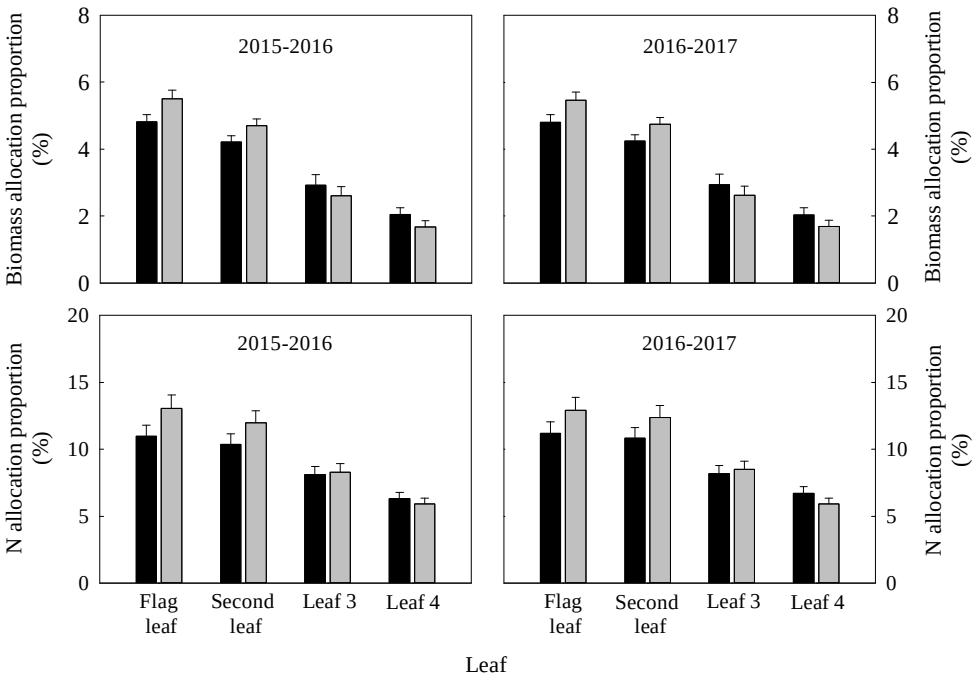

Fig. 3. Biomass and *N* allocation proportion to flag leaf, second leaf, leaf 3, and leaf 4 in per individual winter wheat plant at anthesis over two growing seasons. Vertical bars indicate standard error. Columns as follows: black, 8 October; dark grey, 22 October.

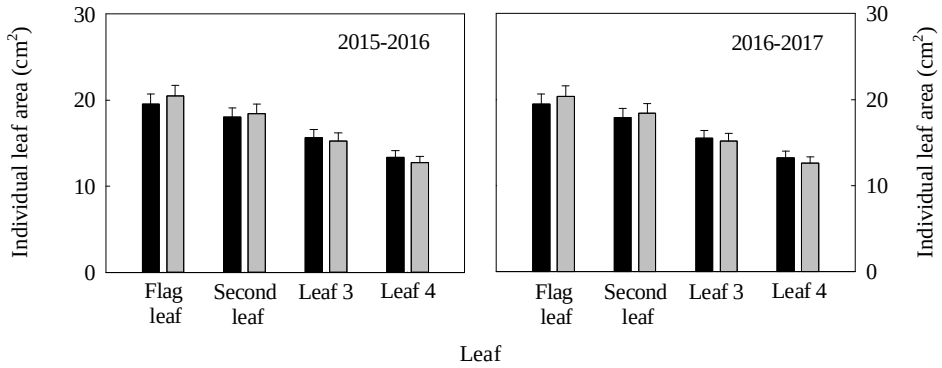

Fig. 4. Area per individual leaf at different positions during anthesis in winter wheat over two growing seasons. Vertical bars indicate standard error. Columns as follows: black, 8 October; dark grey, 22 October.

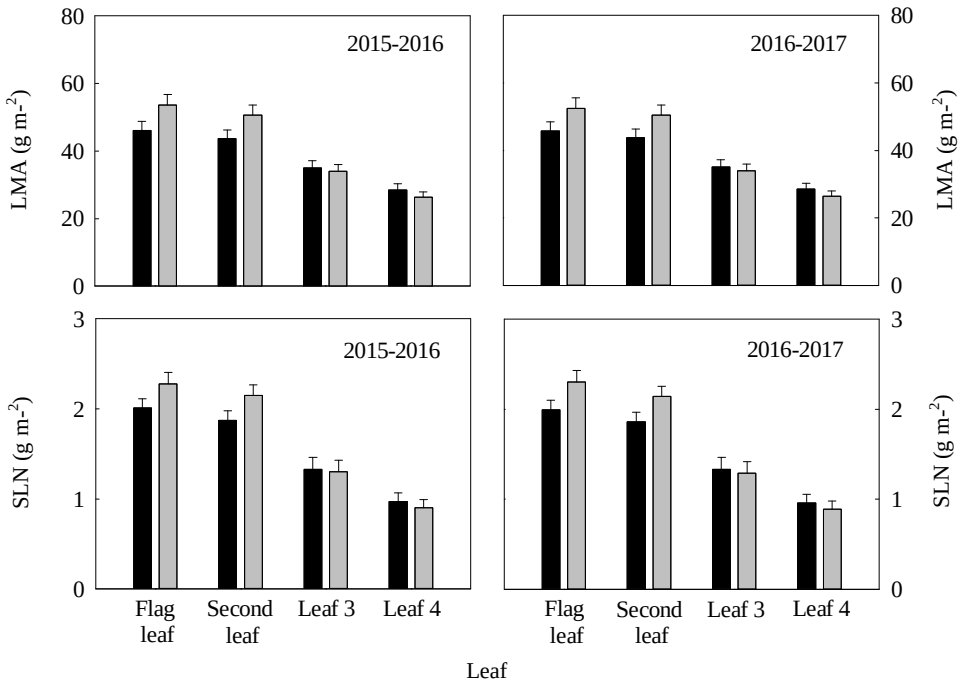

Fig. 5. Leaf mass per area (*LMA*) and specific leaf nitrogen content (*SLN*) of different leaf layers at anthesis in winter wheat over two growing seasons. Vertical bars indicate standard error. Columns as follows: black, 8 October; dark grey, 22 October.

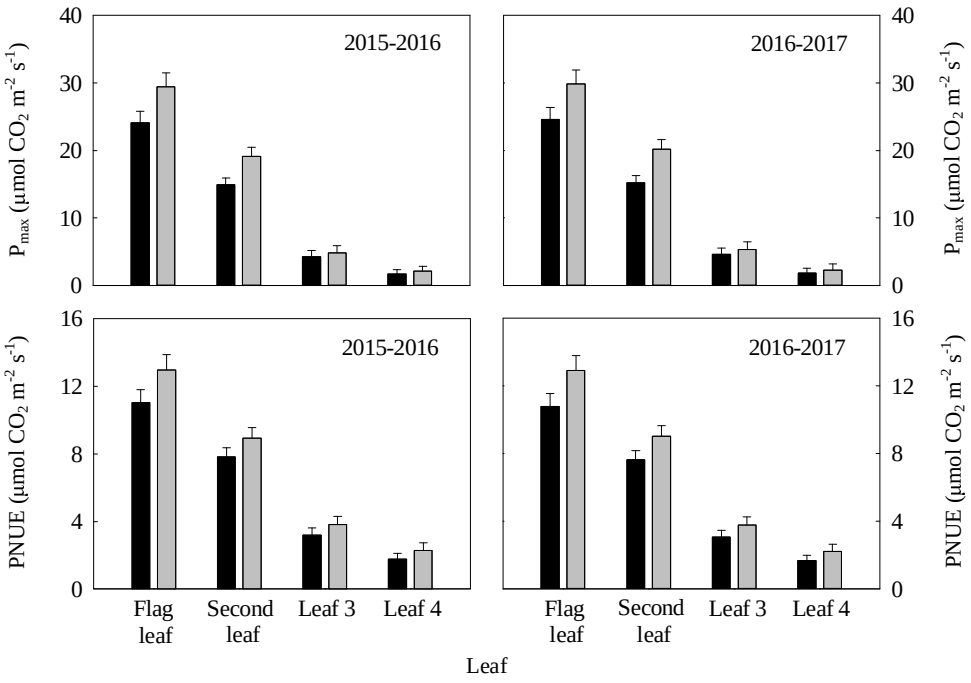

Fig. 6. Light-saturated net photosynthetic rate (P_{max}) and photosynthetic nitrogen use efficiency (*PNUE*) of different leaf layers at anthesis in winter wheat over two growing seasons. Vertical bars indicate standard error. Columns as follows: black, 8 October; dark grey, 22 October.

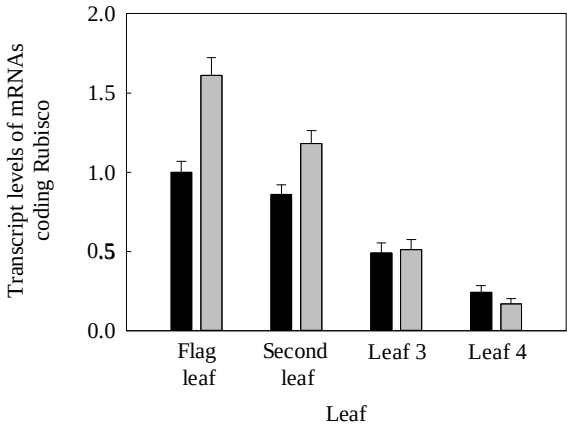

Fig. 7. Transcript levels of *mRNAs* coding Rubisco per unit leaf area of different leaf positions at anthesis in winter wheat during the 2016-2017 season. Vertical bars indicate standard error. Columns as follows: black, 8 October; dark grey, 22 October.

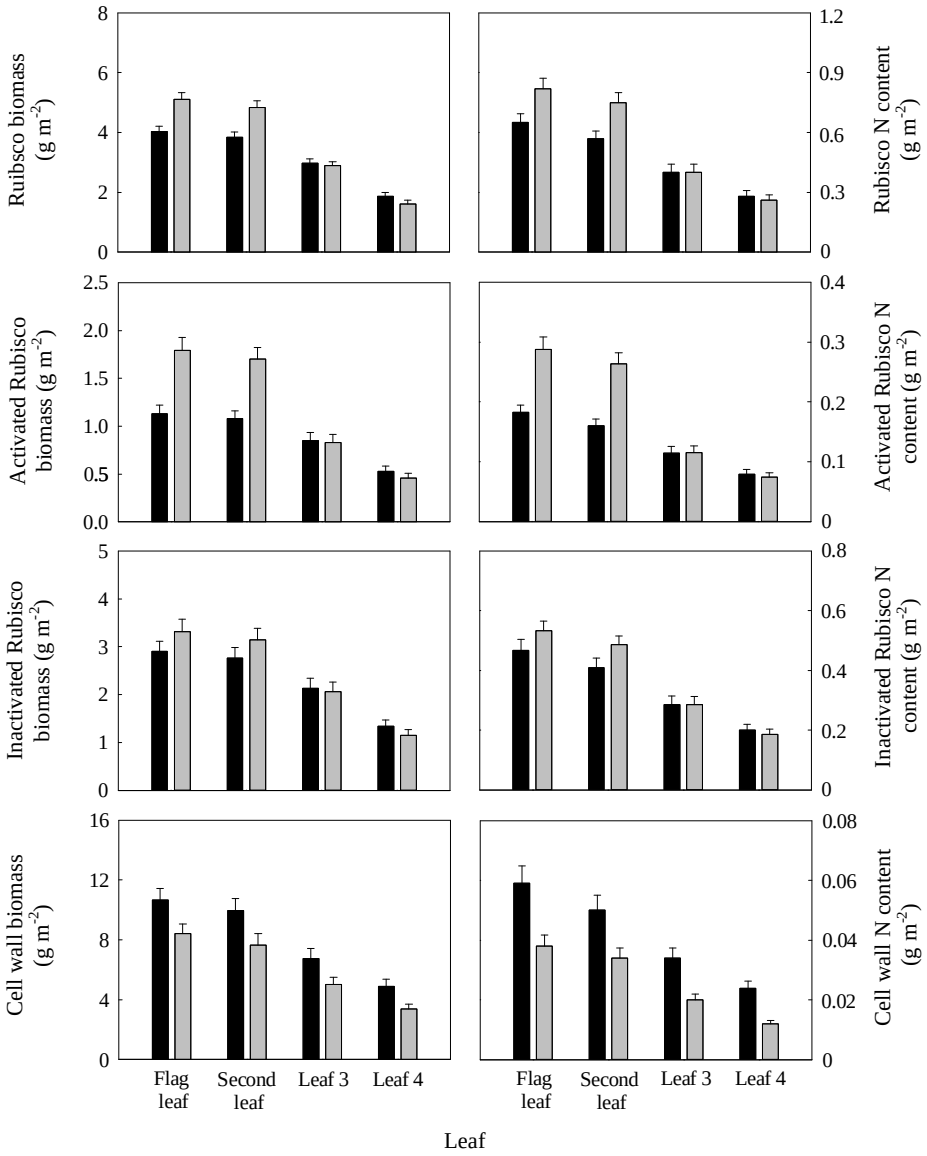

Fig. 8. Rubisco biomass and *N* content, cell wall biomass and *N* content, activated Rubisco biomass and *N* content, and inactivated Rubisco biomass and *N* content per unit leaf area at different leaf positions during anthesis of winter wheat in the 2016-2017 season. Vertical bars indicate standard error. Columns as follows: black, 8 October; dark grey, 22 October.

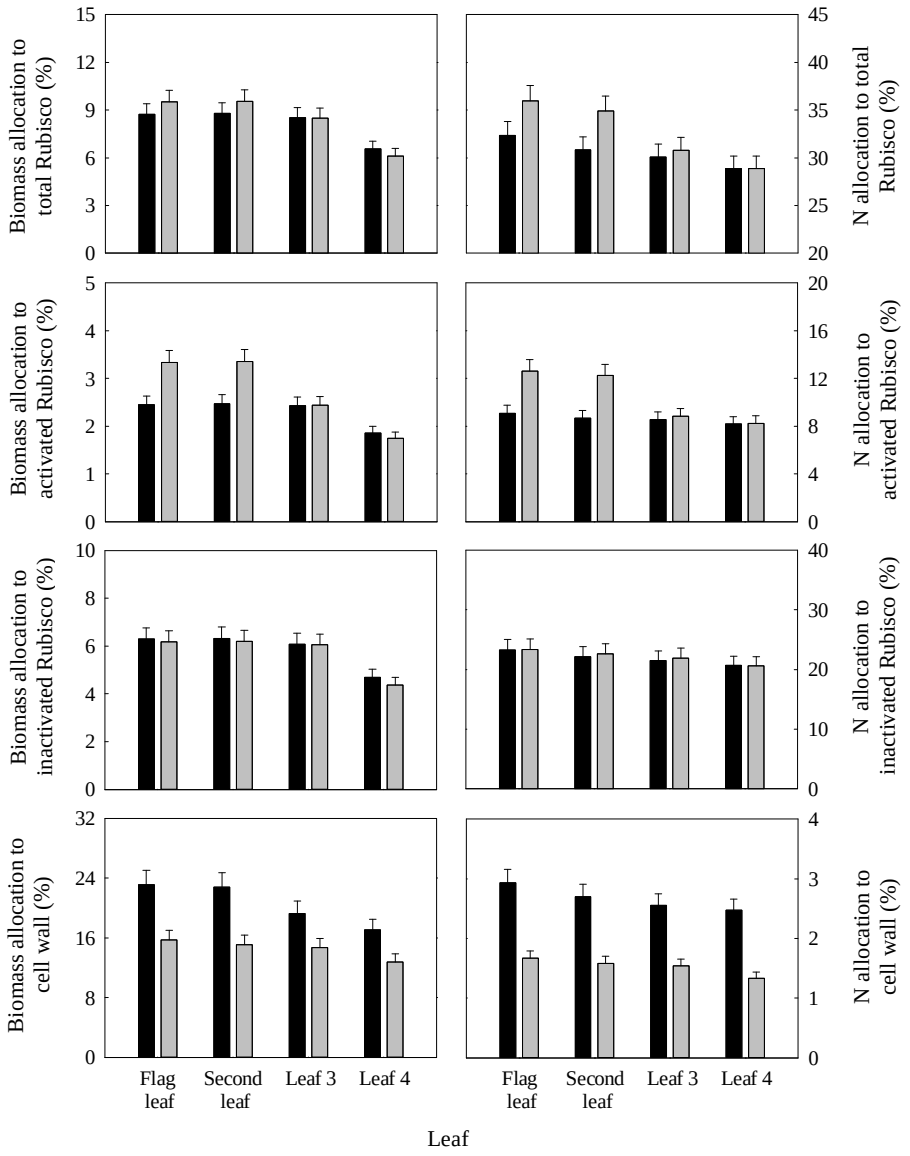

Fig. 9. Biomass allocation to total Rubisco, *N* allocation to total Rubisco, biomass allocation to cell wall, *N* allocation to cell wall, biomass allocation to activated Rubisco, *N* allocation to activated Rubisco, biomass allocation to inactivated Rubisco, and *N* allocation to inactivated Rubisco per unit leaf area of different leaf positions at anthesis of winter wheat during the 2016-2017 season. Vertical bars indicate standard error. Columns as follows: black, 8 October; dark grey, 22 October.

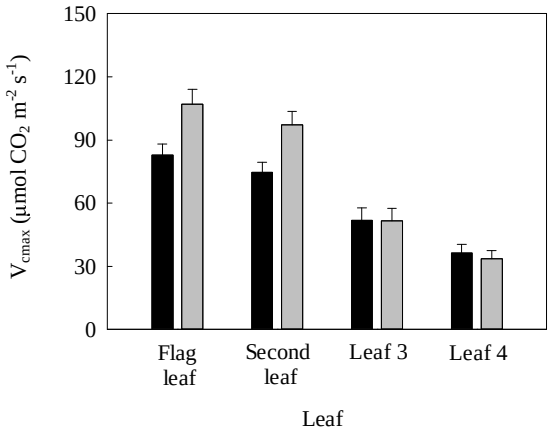

Fig. 10. Maximum carboxylation rate limited by Rubisco (V_{cmax}) per unit leaf area at different leaf positions during anthesis of winter wheat in the 2016-2017 season. Vertical bars indicate standard error. Columns as follows: black, 8 October; dark grey, 22 October.

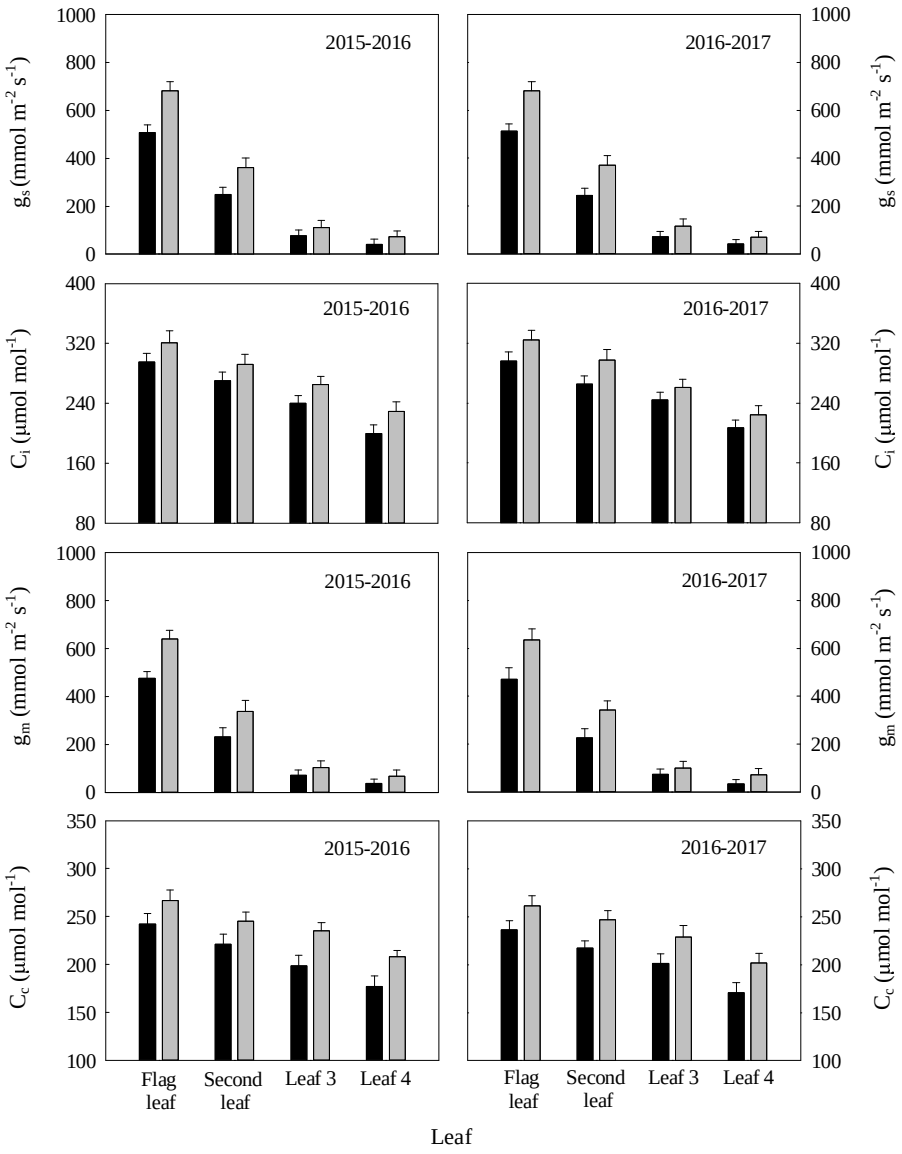

Fig. 11. Stomatal conductance (g_s), intercellular CO_2 concentration (C_i), mesophyll conductance (g_m), and choroplastic CO_2 concentration (C_c) per unit leaf area at different leaf positions during anthesis in winter wheat over two growing seasons. Vertical bars indicate standard error. Columns as follows: black, 8 October; dark grey, 22 October.

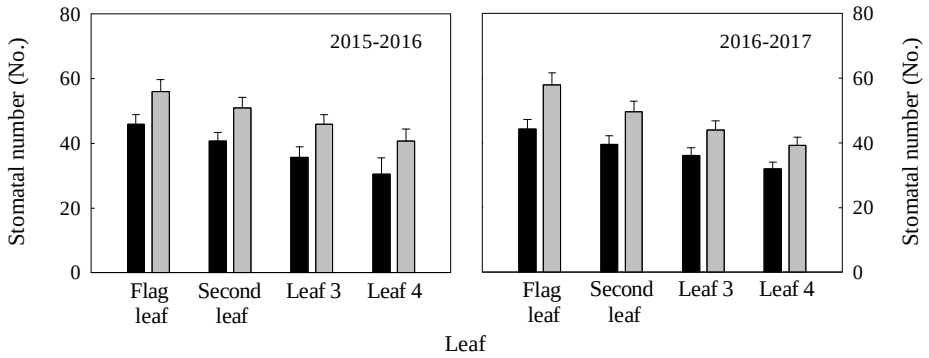

Fig. 12. Stomatal number per unit leaf area at different leaf positions during anthesis in winter wheat over two growing seasons. Vertical bars indicate standard error. Columns as follows: black, 8 October; dark grey, 22 October.

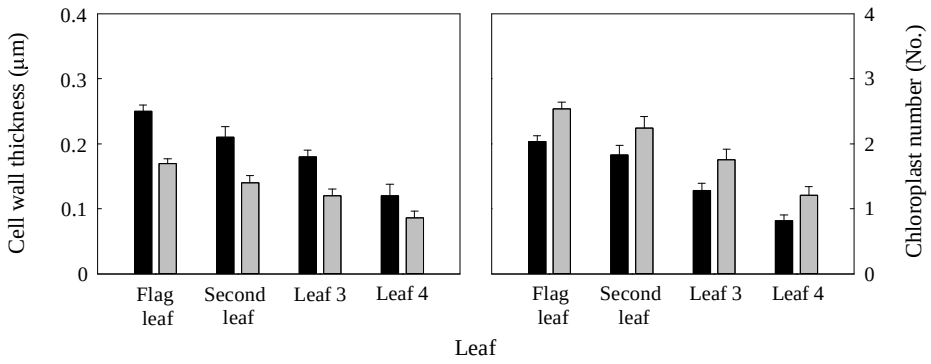

Fig. 13. Cell wall thickness and chloroplast number per unit leaf area at different leaf positions during anthesis of winter wheat in the 2016-2017 season. Vertical bars indicate standard error. Columns as follows: black, 8 October; dark grey, 22 October.

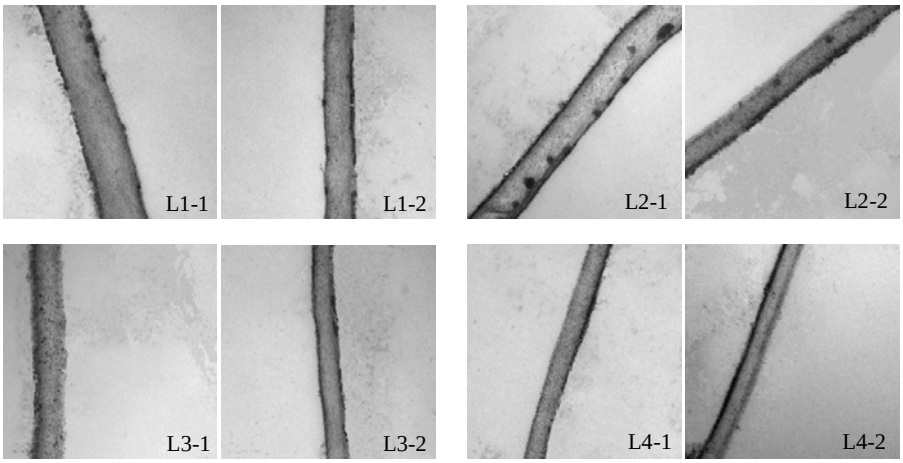

Fig. 14. Estimates of cell wall thickness in winter wheat leaf (L1-1, flag leaf on 8 October; L1-2, flag leaf on 22 October; L2-1, second leaf on 8 October; L2-2, second leaf on 22 October; L3-1, leaf 3 on 8 October; L3-2, leaf 3 on 22 October; L4-1, leaf 4 on 8 October; L4-2, leaf 4 on 22 October) with normal and late sowing at anthesis by electron microscopy in the 2016-2017 season. All pictures are magnified 100,000×.

Table 1. Grain yield, yield components, and nitrogen utilization efficiency (UTE) at harvest for two sowing dates over two wheat growing seasons. Values are means±standard errors of three replicates per treatment.

Season	Sowing date	Grain yield (kg ha^{-1})	Spike number (10^4 ha^{-1})	Grain number per spike	Thousand grain weight (g)	UTE (kg kg^{-1})
2015-2016	8-Oct	9316.7±232.9a	662.4±16.6a	37.2±0.93b	39.5±0.94a	31.4±0.85b
	22-Oct	9243.7±225.1a	590.1±14.7b	41.8±1.1a	39.4±1.0a	34.7±0.92a
2016-2017	8-Oct	9432.8±243.8a	670.5±16.8a	37.6±1.0b	39.2±1.0a	32.3±0.81b
	22-Oct	9378.6±238.6a	605.7±15.3b	41.6±1.2a	39.6±1.1a	36.0±0.86a

Values followed by the same letter within a column and the same season are not significantly different at $P < 0.05$ as determined by the LSD test.